JOURNAL OF THE AMERICAN COLLEGE OF CARDIOLOGY
© 2014 BY THE AMERICAN COLLEGE OF CARDIOLOGY FOUNDATION
PUBLISHED BY ELSEVIER INC.

VOL. 64, NO. 11, 2014
ISSN 0735-1097/$36.00
http://dx.doi.org/10.1016/j.jacc.2014.07.937

Innervation Patterns May Limit Response to Endovascular Renal Denervation

Abraham R. Tzafriri, PhD,* Felix Mahfoud, MD,† John H. Keating, DVM, DACVP,* Peter M. Markham, MS,* Anna Spognardi, BA,* Gee Wong, BS, HT,* Kristine Fuimaono, BS,‡ Michael Böhm, MD,† Elazer R. Edelman, MD, PhD§‖

ABSTRACT

BACKGROUND Renal denervation is a new interventional approach to treat hypertension with variable results.

OBJECTIVES The purpose of this study was to correlate response to endovascular radiofrequency ablation of renal arteries with nerve and ganglia distributions. We examined how renal neural network anatomy affected treatment efficacy.

METHODS A multielectrode radiofrequency catheter (15 W/60 s) treated 8 renal arteries (group 1). Arteries and kidneys were harvested 7 days post-treatment. Renal norepinephrine (NEPI) levels were correlated with ablation zone geometries and neural injury. Nerve and ganglion distributions and sizes were quantified at discrete distances from the aorta and were compared with 16 control arteries (group 2).

RESULTS Nerve and ganglia distributions varied with distance from the aorta ($p < 0.001$). A total of 75% of nerves fell within a circumferential area of 9.3, 6.3, and 3.4 mm of the lumen and 0.3, 3.0, and 6.0 mm from the aorta. Efficacy (NEPI 37 ng/g) was observed in only 1 of 8 treated arteries where ablation involved all 4 quadrants, reached a depth of 9.1 mm, and affected 50% of nerves. In 7 treated arteries, NEPI levels remained at baseline values (620 to 991 ng/g), ≤20% of the nerves were affected, and the ablation areas were smaller (16.2 ± 10.9 mm^2) and present in only 1 to 2 quadrants at maximal depths of 3.8 ± 2.7 mm.

CONCLUSIONS Renal denervation procedures that do not account for asymmetries in renal periarterial nerve and ganglia distribution may miss targets and fall below the critical threshold for effect. This phenomenon is most acute in the ostium but holds throughout the renal artery, which requires further definition. (J Am Coll Cardiol 2014;64:1079–87)

Catheter-based renal sympathetic denervation (RDN) has been introduced as a treatment option for patients with resistant hypertension and has been shown to reduce office and ambulatory blood pressure in open-label registries and randomized, controlled trials (1–6). However, the large-scale, sham-controlled SYMPLICITY HTN-3 (Renal Denervation in Patients With Uncontrolled Hypertension) study recently failed to meet its primary efficacy endpoint (7). In that study, first-generation systems with a single, monopolar radiofrequency (RF) electrode sequentially ablated a series of angularly-staggered endoluminal sites along the renal artery (RA). Procedures were performed

From *CBSET Inc., Lexington, Massachusetts; †Klinik für Innere Medizin III, Kardiologie, Angiologie, und Internistische Intensivmedizin, Universitätsklinikum des Saarlandes, Homburg/Saar, Germany; ‡Biosense Webster, Irwindale, California; §Institute for Medical Engineering and Science, Massachusetts Institute of Technology, Cambridge, Massachusetts; and the ‖Cardiovascular Division, Brigham and Women's Hospital, Harvard Medical School, Boston, Massachusetts. This study was supported in part by a National Institutes of Health grant (R01 GM-49039) to Dr. Edelman and research grants from Cordis/Biosense Webster, Inc., a Johnson & Johnson Company, to CBSET. Drs. Mahfoud and Böhm are supported by Deutsche Hochdruckliga und Deutsche Gesellschaft für Kardiologie; were investigators of the SYMPLICITY HTN-1 and -2 trials; and received research grants, speaker's honorarium, and/or consultancy fees from Medtronic/Ardian, St. Jude Medical, Boston Scientific, and/or Cordis. Ms. Fuimaono is an employee of Cordis/Biosense Webster, Inc., a Johnson & Johnson Company. Dr. Böhm is supported by Deutsche Forschungsgemeinschaft (KFO 196). All other authors have reported that they have no relationships relevant to the contents of this paper to disclose.

Listen to this manuscript's audio summary by *JACC* Editor-in-Chief Dr. Valentin Fuster.
You can also listen to this issue's audio summary by *JACC* Editor-in-Chief Dr. Valentin Fuster.

Manuscript received April 26, 2014; revised manuscript received July 1, 2014, accepted July 7, 2014.

ABBREVIATIONS AND ACRONYMS

NEPI = norepinephrine

RA = renal artery

RDN = renal denervation

RF = radiofrequency

empirically, as there is no intraprocedural test available to assess sufficient wall contact or effective destruction of renal nerves (8). RDN was recommended to commence distally and to be withdrawn by pulling and rotating the catheter tip, and it involved at least 4 focal treatments with a distance of ≥5 mm between each site (9).

SEE PAGE 1088

As the superior aspect of the RA is thought to be especially rich in ganglia and sympathetic nerves, it is recommended to apply the last ablations close to the ostium in a superior position (10). However, ganglia distributions along the RA have not been published, and published nerve mapping (11–13) has relied on coarse segmentation of the RA into proximal, middle, and distal segments that provides little insight into ostial anatomy. We, therefore, performed a similar procedure in Yorkshire swine, quantified the variation of nerve and ganglion size and density with distance from the aorta, and correlated these anatomical features with RF ablation efficacy.

METHODS

ANIMAL MODELS AND EXPERIMENTAL OVERVIEW. All animal experiments were performed at CBSET, Inc. (Lexington, Massachusetts) and adhered to the Guide for the Care and Use of Laboratory Animals (14) under an institutional animal care and use committee-approved protocol. In total, 24 renal arteries from 12 castrated male Yorkshire swine (age 4.5 to 5.0 months) were assessed.

Group 1 consisted of 4 pigs (41.3 to 44.6 kg) undergoing bilateral denervation of the aorta/renal artery with a prototype multielectrode renal crescent catheter (Biosense Webster, Diamond Bar, California) using a custom-designed generator that independently controlled the power of each monopolar electrode and the irrigation rate of room temperature saline (~23°C) through electrode ports. To reduce variability in energy delivery by the monopolar electrodes, ground pads were placed at the same position (between the shoulder blades) in each treated animal. Each treatment was administered under fluoroscopic guidance by up to 3 electrodes (15 W/30 s): 1 at the aortic inlet of the ostium and up to 2 neighboring electrodes deeper within the ostium (**Figure 1**). Electrode dimensions (3 mm) and spacing (4 mm) along with catheter curvature ensured that treatment sites did not extend beyond ~6 mm from the aorta. Animals were euthanized on day 7, and renal arteries and associated aorta were removed *en bloc*, preserving orientation and surrounding tissue. Kidney samples were collected, flash frozen, and shipped for norepinephrine (NEPI) analysis. RA sections at 3 predetermined distances from the aorta were analyzed morphometrically to determine ablation area dimensions and quantify the diameters and locations of nerves and ganglia as detailed in the following text.

Group 2 consisted of 8 pigs (52.1 to 63.2 kg) that did not undergo ostial RDN but were used to analyze nerve and ganglia size and positional distribution at the same 3 distances from the aorta.

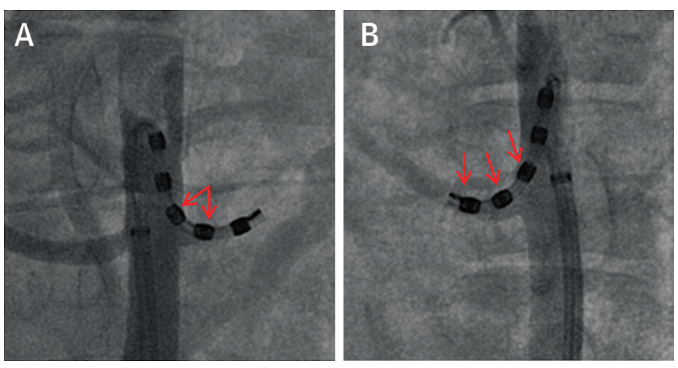

FIGURE 1 Angiographic Confirmation of Electrode Positions Relative to the Ostium

Red arrows denote activated electrodes utilized for 2-electrode treatment **(A)** and 3-electrode treatment **(B)**.

HISTOLOGY OF RAS. Each RA with surrounding tissue was trimmed at intervals of 3 to 5 mm to yield 3 cross sections at the aortic ostium. Anatomic orientation was preserved through tissue harvest and processing (e.g., via inking, tagging, and standardization of embedding and slide generation). One hematoxylin and eosin-stained slide and 1 elastin Masson's trichrome-stained slide were generated per paraffin-embedded section. Immunohistochemical staining for tyrosine hydroxylase and for calcitonin gene-related peptide was performed on a subset of sections. To evaluate for any treatment effects at the aortic ostium of the RAs, a series of 5 sagittal aortic sections was similarly stained and evaluated.

HISTOPATHOLOGY EVALUATION AND NERVE ASSESSMENT OF TREATED ARTERIES. A board-certified veterinary pathologist, using light microscopy, examined the histologic sections of the renal arteries and associated tissue. Tissue ablation, as defined by localized coagulative or necrotic changes, was scored qualitatively, and also quantified using Olympus MicroSuite Biological Suite (Olympus, Center Valley, Pennsylvania). Metrics quantified included

total treatment area, width, and depth (defined relative to the wall/lumen interface). Nerves and ganglia were counted on a quadrant basis, their status with regard to treatment zone was determined, and any nerve changes were characterized as primarily degenerative, necrotic, or chronic/reactive. For each treated RA, the percentages of affected nerves and ganglia were calculated in sections showing evidence of mural treatment.

NERVE AND GANGLION DISTRIBUTIONS. Close to the ostium, there is a splay between the neural plexus and artery that normalizes beyond, and in the distal segment there is a tapering of the vessel. This allowed us to evaluate treatment effects at 3 distances from the aortic ostium (~0.3, ~3.0, and ~6.0 mm) where nerve and ganglia distribution and RA diameter differ. We defined nerve and ganglia locations by their distance from the luminal surface and angle relative to an estimated center of the lumen. Sizes were defined by the largest in-plane diameter. Illustrative maps of nerve and ganglia distributions were generated after shifting each of the individual depths by a representative RA lumen radius of 2.5 mm. As both left and right arteries contributed to the composite map, the orientation of right arterial structures was shifted by 180° to maintain consistent orientation. Maps included overlays of traced ablation areas (also shifted by a representative lumen radius of 2.5 mm). Aortic ostial sections were similarly evaluated, but no nerve treatment effects were present.

KIDNEY BIOANALYSIS (NEPI) AND CORRELATION WITH NERVE EFFECTS. Following euthanasia, kidneys were rapidly harvested and minced on dry ice. Kidneys were homogenized and duplicate aliquots were analyzed for quantification of NEPI content by a high-performance liquid chromatography-mass spectrometry assay using stable isotope-labeled analytes as previously described (15,16). NEPI levels were reported as ng/g renal tissue. The observed monotonic dependence of NEPI on the average percentage of affected nerves (X) was fit to a logistic form:

$$NEPI = NEPI_{\min} + \frac{NEPI_{\max} - NEPI_{\min}}{1 + e^{\frac{X - X_{50}}{Slope}}} \quad [1]$$

Here, $NEPI_{\max}$ is the maximal control NEPI concentration, $NEPI_{\min}$ is the minimal achievable NEPI concentration, X_{50} denotes the percentage of affected nerves that ensure a half-maximal reduction in NEPI, and the value of slope determines the sharpness of the decline.

STATISTICAL ANALYSIS. Experimental values are reported descriptively as mean ± SD. The data fit to Equation 1 was performed using GraphPad Prism 3.01 (GraphPad Software, San Diego, California). Continuous (i.e., radial distance, angle, and size) and discrete (i.e., abundance) nerve/ganglion data were pooled from all vessels and categorized by their distance from the aorta. Pairwise and multiple comparisons were conducted based on data categorization. For all statistical tests, datasets were first assessed for normality using a Shapiro-Wilk test (SigmaPlot 11.0, Systat Software, San Jose, California). For pairwise comparisons, if normality was met, a Student *t* test was conducted; otherwise, a Mann-Whitney rank sum test was performed. For multiple comparisons, if normality was met, a 1-way analysis of variance, Holm Sidak test was performed; otherwise a Kruskal-Wallis 1-way analysis of variance on Ranks, Dunn's test was performed. For all statistical tests, the null hypothesis of no difference was only rejected if the value of the calculated statistic was <0.05 ($p < 0.05$).

RESULTS

PORCINE TREATMENT EFFECTS. Maximal zones of injury were achieved at the RA sections closest to the aorta for all treatments. Maximal ablation zones varied in orientation and shape, and often included or bordered anatomic structures, such as lymph nodes, other large blood vessels, and the hypaxial skeletal muscle. Quantitative morphometry of maximal ablation zones (Table 1) estimated depth (4.5 ± 3.1 mm), width (8.0 ± 4.2 mm), and area (26.6 ± 31.0 mm^2) using the irrigated catheter system.

NEPI levels (Table 1) remained at baseline (16) (620 to 991 ng/g) for 7 of the treated arteries were and only efficaciously reduced (37 ng/g) in the treated RA with maximal ablation area (99.1 mm^2), depth (9.1 mm), and width (15.9 mm). Remarkably, although the maximal ablation zone of the efficacious treatment

TABLE 1 Effects 7 Days Post-Treatment Ordered According to Increasing NEPI Values

Artery	No. of Treating Electrodes	NEPI, ng/g	Affected Nerves, %*	Maximal Depth, mm	Maximal Width, mm	Maximal Area, mm^2
1	2†	37.0	63.6%	9.05	15.92	99.09
2	1	619.9	9.1%	3.68	6.62	13.02
3	2	756.1	0.0%	1.85	11.59	14.14
4	2	822.5	20.0%	1.61	2.73	2.35
5	2	893.1	0.0%	7.13	5.69	19.53
6	2	931.8	19.1%	1.74	4.59	7.06
7	3	954.5	16.7%	7.96	7.31	35.80
8	2‡	990.7	8.3%	2.55	9.70	21.64

*Average (SDs) evaluated over sections with evidence of treatment. †Ostial electrode power = 8.0 W. ‡Ostial electrode power = 7.6 W.
NEPI = norepinephrine.

JACC VOL. 64, NO. 11, 2014
SEPTEMBER 16, 2014:1079–87

involved all 4 quadrants of the section closest to the ostium, only 27.3% of nerves in this section resided in or near the ablation zone and were affected (Figures 2A and 2B). The sole ganglion in this section was beyond the ablation zone and was unaffected. In contrast, more distally from the aorta (~3.0 mm), treatment ablated a smaller area (15.2 mm^2) extending ≤2.1 mm from the lumen, yet 100% of nerves in this section were within or adjacent to the ablation zone and were affected (Figures 2C and 2D). Tyrosine hydroxylase immunostaining of these (Figures 3A and 3B) and neighboring sections confirmed that the majority of nerves within the periarterial region, including the majority of affected nerves, contained notable, diffuse sympathetic components. Calcitonin gene-related peptide immunostaining, indicative of sensory afferent innervation, was sparse and multifocal in affected and unaffected nerves, including within individual nerve bundles.

In the 7 arteries in which no efficacy was observed, maximal ablation areas (Table 1) were smaller (16.2 ± 10.9 mm^2) and restricted to 1 to 2 quadrants at maximal depths of 3.8 ± 2.7 mm, so that no ganglia and fewer than 33% of the nerves at the ostium were affected (Figures 4A to 4D). Although variable nerve distribution precluded correlation of renal NEPI levels with nerve effects at the section closest the ostium, NEPI levels did exhibit a threshold dependence on the percentage of affected nerves as calculated across arterial sections (Figure 5). The data illustrate that nerve ablation in distinct arterial cross sections has an additive effect on renal NEPI, and that efficacious reduction requires an above threshold nerve effect (between 20% to 63% of nerves, and most likely around 50%). To contextualize these findings, we evaluated innervation patterns at 3 distinct distances from the aorta across all arteries (n = 24).

ANATOMY OF PORCINE RA OSTIUM. Nerves and ganglia were located closer to the lumen with increasing distance from the aorta. At the aorta

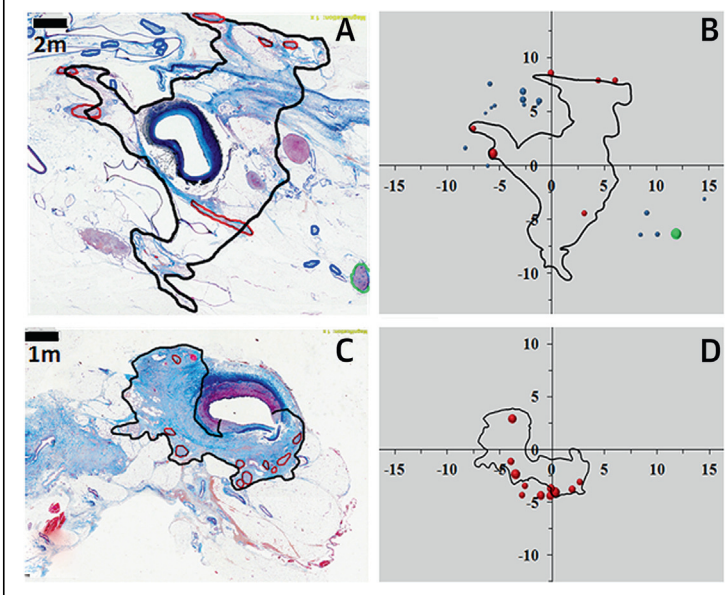

FIGURE 2 Histopathological Appearance of the Norepinephrine-Reducing Ostial Treatment

Treated renal artery sections **(A)** directly at or **(C)** ~3.0 mm away from the aorta with overlaid morphometry: ablation zone **(black line),** affected nerves **(circled red),** unaffected nerves **(circled blue),** and unaffected ganglion **(circled green)**. Standardized comparison is facilitated by overlaying morphometric tracings **(A and C)** onto nerve maps **(B and D)** with a defined, circular lumen (2.5 mm diameter). Orientation is uniform: top = ventral, left = cranial. In **B and D, circle sizes** denote the measured sizes of nerves (**red** = affected, **blue** = unaffected) and ganglia (**green** = unaffected).

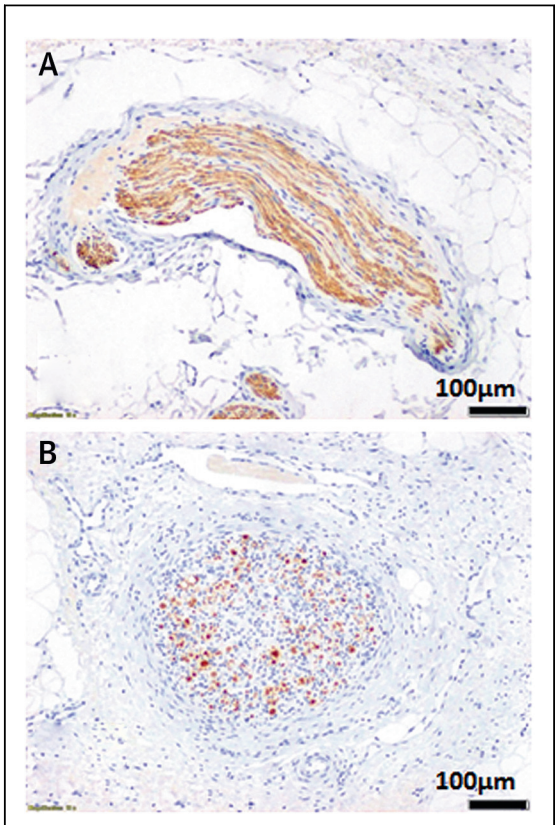

FIGURE 3 Histopathological Appearance of Ostial Sympathetic Nerves

Magnified views of an unaffected nerve from Figure 2A **(A)** and an affected nerve from Figure 2C **(B)**. Tyrosine hydroxylase immunostaining is strong and diffuse in the unaffected nerve **(A)** but patchy and granular in the affected nerve **(B),** which also exhibits hypercellularity and architectural disruption as part of the degenerative and proliferative response to treatment.

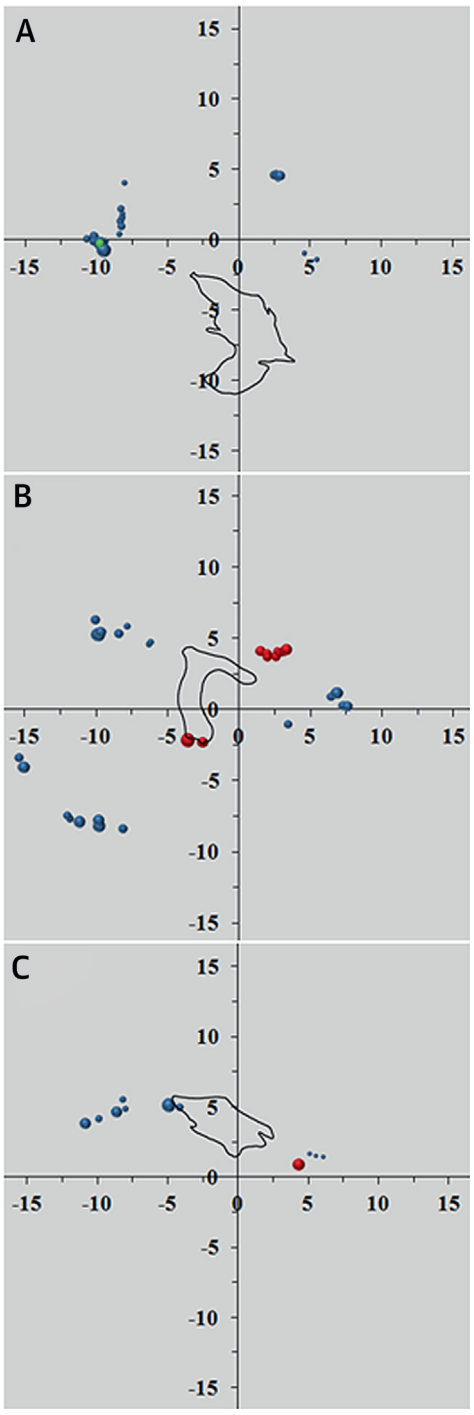

FIGURE 4 Nonefficacious Ostial Ablations

Maximal ablation zones along with nerve and ganglia positions and sizes at the same distance from the aorta (~0.3 mm) are depicted for treatments with norepinephrine levels as follows: 893 ng/g **(A)**, 932 ng/g **(B)**, and 620 ng/g **(C)**. Circle sizes and other figure details as described in Figure 2.

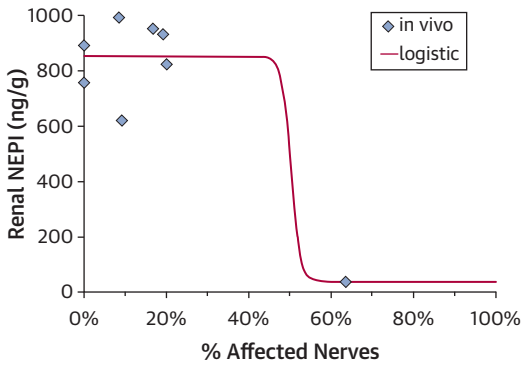

FIGURE 5 Threshold to Biomarker Effect

Norepinephrine (NEPI) levels **(diamonds)** dependence on the percentage of affected nerves in affected arterial sections. A fit of Equation 1 (**red line**, $R^2 = 0.85$) estimates the threshold as 50.3% affected nerves.

(Figure 6A), nerves were localized (i.e., displayed frequency >5%) at radial depths of 2 to 12 mm (median 6.3 mm). At a distance of ~3.0 mm from the aorta (Figure 6B), nerves were localized at radial depths of 2 to 8 mm (median 4.1 mm), whereas at a distance of ~6.0 mm (Figure 6C) nerves localized to radial depths of 1 to 5 mm (median 2.0 mm). These differences were statistically significant ($p < 0.001$) and implied that 75% of nerves were located within 9.3, 6.3, and 3.4 mm of the lumen at the aorta and 3.0, and 6.0 mm into the RA. Ganglion distributions displayed a similar but less pronounced trend, with 75% located within 10.8 mm from the lumen at the aorta versus 7.5 mm ($p < 0.05$) and 8.3 mm ($p < 0.05$) at distances of 3.0 and 6.0 mm from the aorta, respectively.

Circumferential distributions of nerves and ganglia also varied with distance from the aorta, as evidenced by quadrant-level composite maps. At the aorta, nerves and ganglia were more abundant in the superior-posterior and particularly the superior-anterior (e.g., superior ostium) quadrants (Figure 7A), but most were localized at >5 mm from the lumen. At ~3.0 mm from the aorta (Figure 7B), nerves (but not ganglia) were more abundant in the anterior and superior-posterior quadrants, and again most were localized at >5 mm from the lumen. At ~6.0 mm from the aorta (Figure 7C), ganglia (but not nerves) were more abundant in the superior quadrants at >5 mm from the lumen.

Nerve size (Online Table) but not ganglion size exhibited a statistically significant ($p < 0.001$) dependence on distance from the aorta. Average

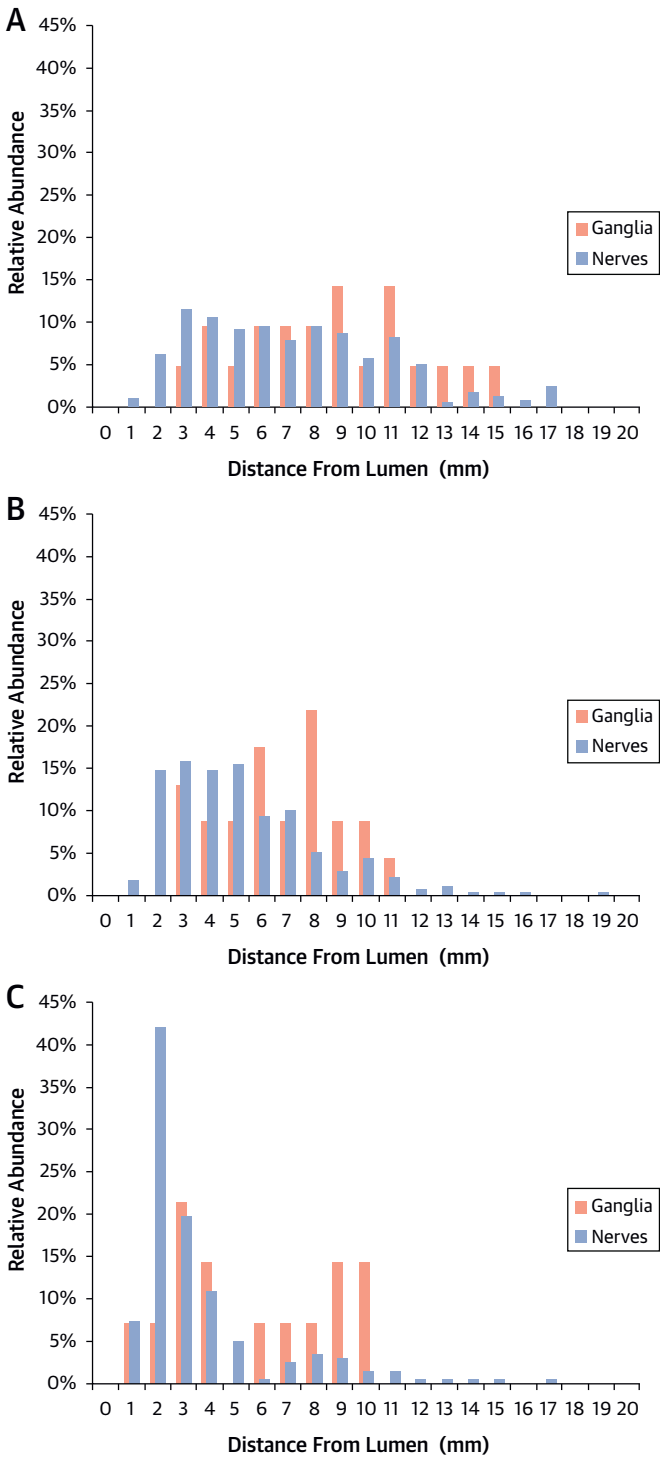

FIGURE 6 The Radial Distributions of Nerves and Ganglia Become More Diffuse Closer to the Ostium

Histograms of the relative abundances of nerves and ganglia are depicted at ostial distances of 0.3 mm **(A),** 3.0 mm **(B),** and 6.0 mm **(C)**. Data from Figures 7A to 7C.

nerve size increased from 165 μm at the aorta to 185 μm at ~3.0 mm and 216 μm at ~6.0 mm.

DISCUSSION

Sympathetic nerve activity contributes to the development and progression of hypertension and some of its comorbidities (17). Catheter-based RDN can reduce sympathetic activity (18) and has been approved in some countries for treatment of resistant hypertension (19). However, pre-clinical data, which would allow us to fully understand the physiology and anatomy of the renal sympathetic nervous system and to guide procedures, are incomplete, leading to anecdotal treatment recommendations. One such procedural recommendation is to intensively treat the RA ostium (9,19), especially the superior part, which is thought to be particularly rich in ganglia and sympathetic nerves. Placement of single electrode catheters in the proximal part of the renal arteries can be challenging and may be unstable and without sufficient wall contact (20,21), raising the question about whether patients really derive benefit from such attempts? Herein, for the first time to our knowledge, we provided quantitative data on nerve and ganglia distribution near the ostium that can help guide the decision as to preferential treatment sites.

Although several trials have shown that RDN can reduce blood pressure (1,5,6,22), the recent blinded, sham-controlled SYMPLICITY HTN-3 trial failed to reach its primary efficacy endpoint, defined as a significant difference in systolic blood pressure between the RDN group and the sham-treated group (7). The procedures were mostly performed using the first-generation single-electrode monopolar catheter systems to deploy RF energy to the vessel wall. One of the major limitations of the available techniques is the absence of intraprocedural tests to assess proper wall contact and effective destruction of the renal sympathetic nerves (8). Indeed, it appears that RDN only lowers blood pressure in certain patients but not in all. Subsequent to the SYMPLICITY HTN trials, nonresponse to RDN was defined as systolic blood pressure reduction of <10 mm Hg 6 months after treatment. However, blood pressure response after RDN varies, and in up to 50% of subjects, blood pressure changes are minor or absent (23). Several causes for clinical nonresponse have been proposed: inappropriate patient selection, changes in adherence during follow-up, minor contribution of sympathetic nerve activity to hypertension, and ineffective procedures. The latter may benefit from catheter refinements and scientifically sound treatment

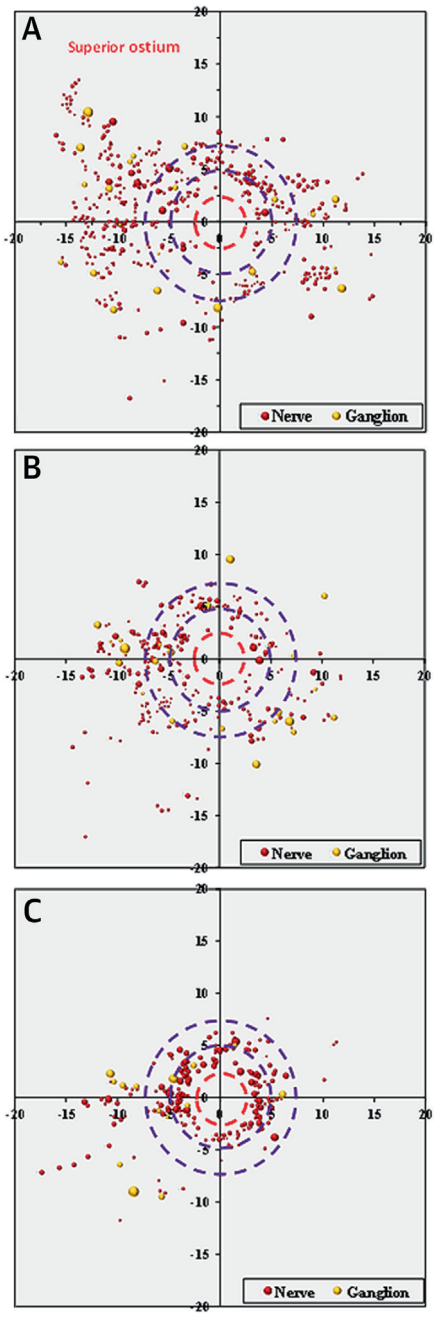

FIGURE 7 Cross-Sectional Nerve and Ganglion Distributions Vary With Distance From the Aorta

Composite polar coordinate distributions are depicted at distances from the aorta: 0.3 mm **(A)**, 3.0 mm **(B)**, and 6.0 mm **(C)**. Nerve and ganglia are depicted by **closed circles** of varying radii based on measured sizes. **Red dashes** depict the location of an idealized lumen. **Purple dashes** depict the locus of points that are 2.5 mm and 5.0 mm away from the lumen. Orientation: **top** = ventral, **left** = cranial.

recommendations. We were able to document for the first time a correlation between NEPI, the biomarker for ablation effects, and the percentage of affected nerves in treated arterial segments. NEPI levels remained at baseline for treatments that affected ≤20% of nerves in the treated segment, as it seems that 50% of nerves must be ablated to achieve half-maximal NEPI reduction.

The variable impact of RDN merits consideration of variability in target anatomy. Nerve density is higher in proximal segments of the renal arteries, although with increasing distance from the aorta, nerve, and ganglia they are localized closer to the lumen. As the average ablation depth of available RF RDN systems is ~3 to 4 mm, our assessment of ostial tissue sections suggests that this anatomic site may be unfavorable for intravascular RDN, contrary to widely-held beliefs. Our study suggests that ostial ablations extending up to 5 mm from the lumen can affect ≤38% of nerves, whereas a 5 mm ablation applied ≥6 mm from the aorta can affect up to 85% of nerves. The efficacy of intravascular RDN within a given RA segment, particularly by single electrodes, is therefore dependent on the circumferential location and depth from the luminal surface of sympathetic nerves and ganglia (Central Illustration). Although our data confirmed that nerves and ganglia are more abundant at the superior ostium, they also show

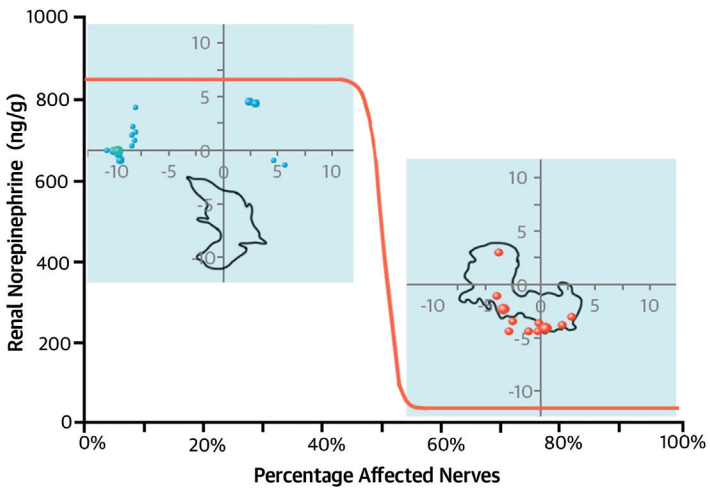

CENTRAL ILLUSTRATION Threshold to Biomarker Effect

Renal norepinephrine levels exhibit a threshold dependence on the percentage of affected nerves **(red circles)**, namely those residing within or at the periphery of the ablation zone **(black line)**. Far from the ablation zones, nerves **(blue circles)** and ganglia **(green circles)** are unaffected.

that excess ablation targets were distributed >5 mm from the lumen, and therefore, were beyond the reach of typical ablations.

STUDY LIMITATIONS. Because the vasculorenal anatomy of pigs is generally similar to that of humans, pigs are considered the preferred animal model of renal denervation (16), but caution is warranted in translating our findings to humans as the renal arteries in young, healthy swine may be different from the renal arteries of long-standing hypertensive patients with respect to calcification, compliance, length, and tortuosity. However, Sakakura et al. (13) recently reported similar trends in human RAs. Based on an analysis of 20 human autopsy subjects (n = 40 renal arteries), they reported that nerves are more abundant in the proximal versus distal segments (40/section vs 34/section, p = 0.03) but also more distant from the lumen (50th percentile: 2.84 vs. 1.81 mm; 75th percentile: 4.67 vs. 3.24 mm). Although this trend is similar to our own findings up to 6 mm from the aorta, Sakakura et al. (13) observed statistically equivalent nerve distributions in proximal and middle segments. This difference in the sensitivity of nerve distribution to the distance from the aorta speaks to the greater resolution provided by our finer segmentation along the length of the animal artery and that arteries in the pig are not alerted by concomitant long-standing hypertension.

CONCLUSIONS

RDN therapies, which assume symmetric neural networks, run the real risk of missing nerves when unitary lesions are imposed. This is especially true for the renal ostium which, although an attractive target, imposes significant challenges. Ganglia and nerves are more abundant at the renal ostium but are located farther from the lumen and are present in all 4 quadrants, not just the superior aspect. Penetration depths, which ablate along the length of the RA, are ineffective at the ostium. As we move forward with this emerging technology, we need to match treatment strategies with increasing understanding of the target anatomy.

REPRINT REQUESTS AND CORRESPONDENCE: Dr. Abraham R. Tzafriri, CBSET Inc., 500 Shire Way, Lexington, Massachusetts 02421. E-mail: rtzafriri@cbset.org.

PERSPECTIVES

COMPETENCY IN MEDICAL KNOWLEDGE: Sympathetic nerve activity contributes to hypertension and its comorbidities, but the response to catheter-based RDN has been variable in studies conducted to date.

TRANSLATIONAL OUTLOOK: More detailed knowledge of RA innervation patterns derived from animal models might be useful in guiding interventions in patients with hypertension to yield more consistent antihypertensive effects.

REFERENCES

1. Mahfoud F, Ukena C, Schmieder RE, et al. Ambulatory blood pressure changes after renal sympathetic denervation in patients with resistant hypertension. Circulation 2013;128:132–40.

2. Kaiser L, Beister T, Wiese A, et al. Results of the ALSTER BP real-world registry on renal denervation employing the Symplicity system. EuroIntervention 2014;10:157–65.

3. Persu A, Azizi M, Burnier M, Staessen JA. Residual effect of renal denervation in patients with truly resistant hypertension. Hypertension 2014;62:450–2.

4. Ott C, Mahfoud F, Schmid A, et al. Renal denervation in moderate treatment-resistant hypertension. J Am Coll Cardiol 2013;62:1880–6.

5. Esler MD, Krum H, Schlaich M, Schmieder RE, Bohm M, Sobotka PA. Renal sympathetic denervation for treatment of drug-resistant hypertension: one-year results from the Symplicity HTN-2 randomized, controlled trial. Circulation 2012;126:2976–82.

6. Krum H, Schlaich MP, Bohm M, et al. Percutaneous renal denervation in patients with treatment-resistant hypertension: final 3-year report of the Symplicity HTN-1 study. Lancet 2014;383:622–9.

7. Bhatt DL, Kandzari DE, O'Neill WW, et al. A controlled trial of renal denervation for resistant hypertension. N Engl J Med 2014;370:1393–401.

8. Mahfoud F, Bhatt DL. Catheter-based renal denervation: the black box procedure. J Am Coll Cardiol Intv 2013;6:1092–4.

9. Bertog SC, Blessing E, Vaskelyte L, Hofmann I, Id D, Sievert H. Renal denervation: tips and tricks to perform a technically successful procedure. EuroIntervention 2013;9 Suppl R:R83–8.

10. Tsioufis C, Mahfoud F, Mancia G, et al. What the interventionalist should know about renal denervation in hypertensive patients: a position paper by the ESH WG on the interventional treatment of hypertension. EuroIntervention 2014;9:1027–35.

11. Atherton DS, Deep NL, Mendelsohn FO. Micro-anatomy of the renal sympathetic nervous system: a human postmortem histologic study. Clin Anat 2011;25:628–33.

12. Tellez A, Rousselle S, Palmieri T, et al. Renal artery nerve distribution and density in the porcine model: biologic implications for the development of radiofrequency ablation therapies. Transl Res 2013;162:381–9.

13. Sakakura K, Ladich E, Cheng Q, et al. Anatomical distribution of human renal sympathetic nerves: pathologic study. J Am Coll Cardiol 2014;63:A2151.

14. NRC (National Research Council). Guide for the Care and Use of Laboratory Animals. Washington, DC: National Academy Press, 1996.

15. Ji C, Walton J, Su Y, Tella M. Simultaneous determination of plasma epinephrine and norepinephrine using an integrated strategy of a fully automated protein precipitation technique,

reductive ethylation labeling and UPLC-MS/MS. Anal Chim Acta 2010;670:84–91.

16. Sakakura K, Ladich E, Edelman ER, et al. Methodological standardization for the preclinical evaluation of renal sympathetic denervation. J Am Coll Cardiol Intv http://dx.doi.org/10.1016/j.jcin.2014.04.024.

17. Esler M. Renal denervation for hypertension: observations and predictions of a founder. Eur Heart J 2014;35:1178–85.

18. Hering D, Lambert EA, Marusic P, et al. Renal nerve ablation reduces augmentation index in patients with resistant hypertension. J Hypertens 2013;31:1893–900.

19. Mahfoud F, Luscher TF, Andersson B, et al. Expert consensus document from the European Society of Cardiology on catheter-based renal denervation. Eur Heart J 2013;34:2149–57.

20. Hutchinson BD, Keane D, Dodd JD. Renal sympathetic denervation: MDCT evaluation of the renal arteries. AJR Am J Roentgenol 2013;201:W342–6.

21. Shirali AS, Bischoff MS, Lin HM, et al. Predicting the risk for acute type B aortic dissection in hypertensive patients using anatomic variables. J Am Coll Cardiol Img 2013;6:349–57.

22. Worthley SG, Tsioufis CP, Worthley MI, et al. Safety and efficacy of a multi-electrode renal sympathetic denervation system in resistant hypertension: the EnligHTN I trial. Eur Heart J 2013;34:2132–40.

23. Ukena C, Cremers B, Ewen S, Bohm M, Mahfoud F. Response and non-response to renal denervation: who is the ideal candidate? EuroIntervention 2013;9 Suppl R:R54–7.

KEY WORDS aortic tortuosity, renal denervation, superior ostium

APPENDIX For a supplemental table, please see the online version of this article.